Progress in Additive Manufacturing (2022) 7:683–698
https://doi.org/10.1007/s40964-021-00254-7

FULL RESEARCH ARTICLE

The influence of the energy density on dimensional, geometric, mechanical and morphological properties of SLS parts produced with single and multiple exposure types

A. C. Lopes[1,2] · A. M. Sampaio[1,2,3] · A. J. Pontes[1,2]

Received: 7 August 2021 / Accepted: 13 December 2021 / Published online: 26 January 2022

Abstract
Selective Laser Sintering (SLS) is a Powder Bed Fusion technology that embraces a large number of variables influencing the properties of the parts produced. The well-known dependence and complex interaction established between the main process parameters demands continuous empirical research for effective SLS monitoring. The assessment of the energy density supplied by the laser beam to the powder bed during the process, that depends on the combination of the laser power, hatch distance, scan speed and layer thickness, is frequently considered for that purpose. Therefore, this research intends to evaluate the influence of the energy density on the dimensional, geometric, mechanical and morphological properties of SLS parts produced with conventional Polyamide 12 material. In this study, we considered different hatching and contour parameters in the energy range between 0.158 J/mm^3 and 0.398 J/mm^3 through single and multiple exposure types defining individual and combined parameterization sets, respectively. Results from X-ray computed tomography, tensile tests and scanning electron microscopy show that the implementation of a skin/core configuration allows the production of SLS parts with a valuable set of properties, minimizing the trade-off between mechanical strength and overall accuracy.

Keywords Additive manufacturing · Selective Laser Sintering · Process parameters · Energy density · Polyamide 12

1 Introduction

Selective Laser Sintering (SLS) is an additive manufacturing (AM) technology that belongs to the Powder Bed Fusion (PBF) category [1]. The production of the polymeric parts occurs under controlled environment and encompasses three fundamental stages: (i) spread of powder material along a building platform, (ii) sintering of powder material according to the cross-section of the part through a laser source and (iii) repetition of the process, layer-by-layer, until the whole production of the part [2, 3]. This sequence of events makes the PBF processes, in which SLS is embraced, dependent on a large number of process parameters with significant influence on the sintering process and properties of the parts, including parameters related to the material (e.g., type of material, particles size and shape, mixture ratio), to the temperatures (e.g., preheating temperature, process temperature), to the laser beam (e.g., laser power, beam offset), to the scanning (e.g., scan speed, hatch distance, scan pattern) and to the part (e.g., position, orientation) [4–7]. For process optimization, these parameters are frequently evaluated through the quantification of the thermal energy supplied by the laser beam to the powder bed, as opposed to an individual analysis of the input variables [8–10]. The thermal energy provided during the sintering process depends on key process parameters and directly quantifies the degree of particle melt, the inter-particle coalescence and the microstructural and mechanical properties of SLS parts [3, 8, 11, 12]. A number of different concepts of energy obtained from experimental and/or numerical methods contemplating different assumptions and simplifications have already been proposed in literature. Focusing on experiments conducted with conventional polymeric materials, the energy density by unit of area (ED_A), energy density by unit of volume

✉ A. C. Lopes
acarinalopes@dep.uminho.pt

1 IPC – Institute for Polymers and Composites, University of Minho, Guimarães, Portugal

2 DONE Lab – Advanced Manufacturing of Products and Tools, University of Minho, Guimarães, Portugal

3 Lab2PT, School of Architecture, University of Minho, Guimarães, Portugal

(ED_V) and total energy density (ED_T) are three of the most common [10]. ED_A is a function of the laser power (P_{Laser}), scan speed (S_{Scan}) and hatch distance (D_{Hatch}), respectively, related to the intensity, duration and number of times that the laser acts on the surface of the powder bed (Eq. (1)) [8, 13]:

$$ED_A = \frac{P_{Laser}}{S_{Scan} \times D_{Hatch}} \quad (1)$$

ED_V is an extension of ED_A. It includes the layer thickness (t_{Layer}), a process parameter with a well-known influence on the building time and surface roughness of the parts (Eq. (2)) [10, 14, 15]:

$$ED_V = \frac{P_{Laser}}{S_{Scan} \times D_{Hatch} \times t_{Layer}} \quad (2)$$

In turn, ED_T includes the energy provided during the preheating phase, depending on the specific heat capacity (c_p) and density (ρ) of the material (Eq. (3)) [10]:

$$ED_T = ED_V + c_p \times \rho \times T_{Preheating} \quad (3)$$

All of these parameters play a crucial role during the SLS process. In general terms, previous research proved that when they are combined to define increased values of energy, the inter-particle coalescence is improved and the resulting parts present high density, low porosity, and great mechanical properties [16, 17]. However, when the energy is increased above a critical high value, a considerable amount of surrounding powder particles is sintered to the surface of the parts through heat conduction, causing a phenomenon known as secondary sintering [18, 19]. One of the main observations is the oversizing of parts which can be beneficial to contradict effects of shrinkage when the secondary sintering occurs to a small extent but undesirable for dimensional accuracy when it takes place to a large extent [20]. This demonstrates that medium–low values of energy are advantageous for some properties whereas medium–high values are beneficial for others, requiring a trade-off between accuracy and mechanical performance [18, 19]. Under intensive exposure of the laser beam operating with extremely high levels of energy, the material is susceptible to degrade, resulting in yellowness parts with large voids, low density, high shrinkage and reduced mechanical strength [17, 21–24].

Regardless of the concept of energy, most of the research conducted in this field with conventional polymeric materials is focused on a single set of process parameters, meaning that only one set of variables is considered for analysis. However, the sintering process and the final properties of SLS parts are influenced to a different extent by parameters defining their internal and external layers (i.e., hatching and contour parameters, respectively) [9]. Although these parameters induce similar effects on the parts, the hatching settings have a predominant impact on their properties due to the larger volume that it defines, demanding higher process requirements [9, 25]. The value of energy is also dependent on the properties of the polymeric material, building orientation and direction of the surfaces of the part [10, 16, 26, 27]. Regarding the building orientation, it is known that the properties of parts horizontally and vertically produced stabilize at different levels of energy, depending on the area of the corresponding cross-section [8, 10, 16]. For the same values of energy, parts horizontally produced tend to present greater overall performance until a high level where it becomes less dependent on the building orientation [10, 16]. In fact, this multiplicity of factors restricts a trivial definition of the optimum value of energy for each sintering process. Because of that, the evaluation of fundamental SLS process parameters using the concept of energy density requires continuous research for specific laser-sintering machines and materials [28]. In this regard, Table 1 summarizes some recommended ED_A and ED_V values to successfully process pure polyamide powders in different commercial SLS equipment. This review demonstrates that suitable values of energy are commonly quantified through empirical data that are specific on the equipment and experimental protocol implemented.

The purpose of this research is to provide an in-depth understanding of the influence of fundamental SLS process parameters on the dimensional, geometric, mechanical and morphological properties of the parts produced. Since this AM technology requires a laser source and critical thermal control for the sintering, the analysis was based on the concept of energy density by unit of volume, ED_V, according to Eq. (2). To this aim, a series of hatching and contour parameters were used to define the internal and external layers of the parts, respectively, that were further evaluated through single and multiple exposure types. The single exposure type allowed the production of parts with one set of process parameters, while the multiple exposure type allowed the production of parts with two different sets implementing a skin/core configuration.

2 Materials and methods

An EOS P 396 laser-sintering machine operating with a neat PA12 material (i.e., the PA2200 supplied by EOS GmbH) in a standard mixture ratio of 50:50% was considered for this research. This mixture ratio of virgin and processed material was selected to ensure an efficient packaging and the greatest overall mechanical properties [38]. The experimental methodology of this work was divided into three main phases: (i) the individual analysis of hatching parameters, (ii) the individual analysis of contour parameters, and (iii) the combined analysis of skin/core parameters. In the initial phase, ED_V values ranging between 0.158 to 0.398 J/mm^3 (in

Table 1 ED_A and ED_V values for pure polyamide materials processed by SLS

SLS equipment	Material	ED_A (J/mm^2)	ED_V (J/mm^3)	Reference
Sinterstation 2500 Plus	DuraForm PA12	> 0.012	N/A	[16]
EOS P 380	EOS PA 2200	> 0.010 < 0.048	N/A	[27]
EOS P 380	EOS PA 2200	0.027	N/A	[29]
N/A	DuraForm PA12	0.020–0.080	N/A	[30]
Formiga P 100	EOS PA 2200	0.050	N/A	[31]
Sinterstation 2500 Plus	DuraForm PA12	N/A	> 0.091	[32]
Sinterstation 2500 HS	EOS PA 2200	N/A	0.350–0.400	[33]
N/A	DuraForm PA12	0.020 – 0.100	N/A	[34]
Sinterstation 2500 Plus	DuraForm PA12	0.025	N/A	[35]
Sinterstation 2500 HS	EOS PA 1101	N/A	0.400–0.580	[36]
EOS P 395	EOS PA 2200	N/A	0.370 (0º parts) 0.460 (90º parts)	[10]
Formiga P 100	EOS PA 2200	0.057	N/A	[37]

Table 2 Hatching parameters considered for the experiments

Laser beam strategy	t_{Layer} (mm)	P_{Laser} (W)	D_{Hatch} (mm)	S_{Scan} (mm/s)	ED_V (J/mm^3)
XY-A	0.12	17.10	0.30	3000	0.158
XY-A	0.12	32.00	0.30	4500	0.198
XY-A	0.12	32.00	0.30	3730	0.238
XY-A	0.12	32.00	0.30	2800	0.318
XY-A	0.12	38.70	0.30	3000	0.358
XY-A	0.12	43.00	0.30	3000	0.398
X	0.12	32.00	0.30	2800	0.318
Y	0.12	32.00	0.30	2800	0.318
XY-S	0.12	32.00	0.30	2800	0.318

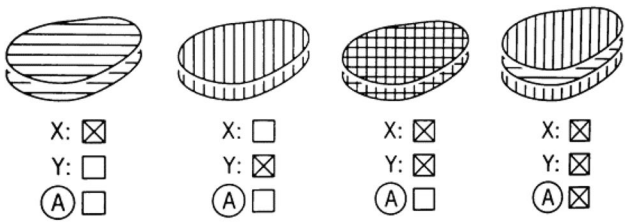

Fig. 1 X, Y, XY-S and XY-A strategies of the laser beam (Adapted from [39])

constant intervals of 0.04 J/mm^3) were evaluated, through the definition of specific combinations of P_{Laser}, S_{Scan}, D_{Hatch} and t_{Layer}, with the laser beam working in the conventional *xy*-alternating-direction (XY-A) (Table 2). Other strategies of the laser beam path were also assessed, including the *x*-direction (X), *y*-direction (Y) and *xy*-simultaneous-direction (XY-S) (Fig. 1). The parameters related to the contour, edges and processing temperatures remained fixed in the standard mode.

In the second phase, the contour parameters were evaluated through different combinations of P_{Laser} and S_{Scan} supplied in a same extent to the top and bottom surfaces of the parts, considering an optimized hatching set. This allowed the analysis of a range between 0.007 and 0.015 J/mm (in constant intervals of 0.002 J/mm) (Table 3).

In the end, an advanced parameterization mode was used to apply two different exposure types in the same part to maximize its mechanical strength through the core, ensuring the dimensional and geometric accuracy of features in smooth surfaces through the skin. Based on the results obtained from the previous phases, a promising combination of hatching and contour parameters was defined considering the thickness of the skin (t_{Skin}) varying 20%, 30% and 40% of the thickness of the part (t_{Part}) (Table 4).

In all experiments, the test specimens required for dimensional, geometric, mechanical and morphological characterization were horizontally produced in the center of the building platform minimizing the influence of the thermal gradients created during the sintering. The corresponding

Table 3 Contour parameters considered for the experiments

Contour parameters		
P_{Laser} (W)	S_{Scan} (mm/s)	P_{Laser}/S_{Scan} (J/mm)
30	3000	0.007
38	3000	0.009
34	3000	0.011
34	2000	0.013
34	4000	0.015
Optimized hatching set (Fixed)		
Strategy	t_{Layer} (mm)	P_{Laser} (W)
Y	0.12	32
D_{Hatch} (mm)	S_{Scan} (mm/s)	ED_V (J/mm^3)
0.3	2800	0.318

exposure types were defined in the EOS PSW 3.8 software, selecting the path *No_Exposure → _Default_EOS* for the individual analysis and *No_Exposure → SkinCore* for the combined analysis. After the sintering process, the test specimens were cleaned with compressed air and sand blasting and then stored in a room with a controlled environment of 22 ºC and 40 rH% until testing.

2.1 Characterization tests

The macro and micro-scale tests used to characterize the test specimens produced with different parameterization modes are described in this section. After testing, the results were statistically treated through a normality test (i.e., Anderson–Darling type) combined with an outlier test (significance level: 0.05), using the basic statistics tools of the Minitab software, to ensure a normal distribution of the data.

2.1.1 Dimensional and geometric accuracy

An artifact test developed by the National Institute of Standards and Technology (NIST) covering a large number of different features (e.g., holes, fine pins, cylinders, staircases) was used in this research to evaluate the limitations and capabilities of SLS to produce parts with dimensional and geometric accuracy (Fig. 2) [40].

The artifact test was measured by X-Ray Computed Tomography (CT) in a ZEISS METROTOM 800 225 kV equipment ($\pm(0.0035+L/100)$ µm) using the METROTOM OS software. The CT images were taken with 120 kV and 1000 µA, considering 2500 projections. The dimensional and geometric characteristics were evaluated through a minimum of five measurements per feature using the INSPECT-plus software according to the criteria and measurement rules proposed by NIST. These five measurements were taken to estimate the standard deviation of the position of the points acquired in the CT images, to reduce the influence of the irregularities of the surfaces on the uncertainty of the measurements.

2.1.2 Mechanical properties

The mechanical properties, such as the elastic modulus, tensile strength, tensile stress at yield (0.2% offset), tensile stress at break, tensile strain at yield and tensile strain at break, were determined through uniaxial tensile tests. Five test specimens per condition, type 1BA (ISO 527-2) (Fig. 3), were tested at 10 mm/min in an Instron 5969 Universal Testing System (with video extensometer) operating with a load-cell of 50 kN at room temperature [41].

2.1.3 Morphological properties

Scanning Electron Microscopy (SEM) analyses were performed in a Nano SEM FEI Nova 200 equipment to evaluate the microstructure, content of porosity and consolidation of powder particles of the test specimens produced with the single and multiple exposure types. Before the measurements, the test specimens were cryogenically cut and prepared with 15 nm of gold coating. The images of the cross-section were obtained with an acceleration voltage of 10 kV.

3 Results and discussion

Substantial modifications in the surface finishing, accuracy of fine pins and holes, mechanical performance and morphological structure of the parts were detected, in function of the process parameters selected for the sintering. This section covers the analysis of the most relevant results obtained from the experiments in respect of the single exposure type of hatching parameters, single exposure type of contour

Table 4 Skin/core parameters considered for the experiments

Skin parameters			Core parameters			Skin/core ratio		
Hatching Strategy	ED_V (J/mm^3)	Contour P_{Laser}/S_{Scan} (J/mm)	Hatching Strategy	ED_V (J/mm^3)	Contour P_{Laser}/S_{Scan} (J/mm)	t_{Skin}/t_{Part} (%)		
X	0.198	0.007	Y	0.318	0.007	20	30	40

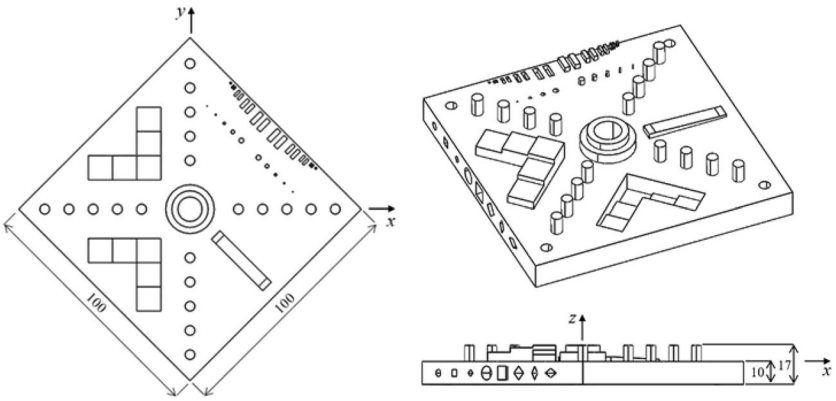

Fig. 2 Artifact test for dimensional and geometric evaluation (dimensions in mm)

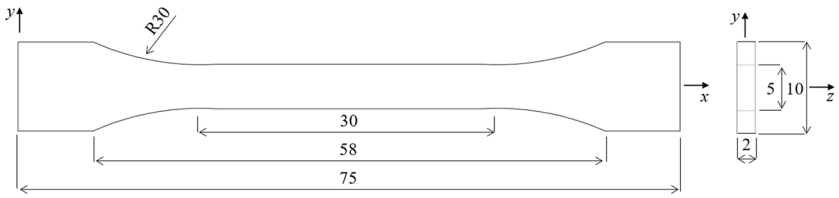

Fig. 3 Test specimen for mechanical analysis (dimensions in mm)

parameters and multiple exposure type using a skin/core configuration.

3.1 Single exposure type of hatching parameters

3.1.1 Description of observations

The primary qualitative analysis of the artifacts test produced with a single exposure type demonstrated the significant influence of the hatching parameters on the quality of the surfaces and features. In a first observation, it was found that low ED_V values are desirable for the manufacturing of fine holes but undesirable for the manufacturing of fine pins in surfaces at 0º directed to the top (Fig. 4).

In turn, the artifacts test produced with high ED_V values (i.e., above 0.318 J/mm^3), presented pronounced problems of cleaning, surface quality and accuracy of details, influencing the holes, fine features and edges (Fig. 5). This was a clear consequence of the heat conduction empowered by high values of energy which intensified the thermal gradients in the powder bed and the secondary sintering of the surrounding powder particles.

The artifacts test produced with the laser beam operating with the X, Y and XY-A strategies revealed similar qualitative outputs. On the other hand, the simultaneous action of the laser beam in both *x* and *y*-directions using the XY-S strategy resulted in non-conforming parts with the full-sintering of holes, loss of precision, poor edges, oversizing and surface roughness. In consequence of the intensive exposure of the laser beam, the artifacts test produced with 0.358 J/mm^3, 0.398 J/mm^3 and XY-S were not considered for the dimensional and geometric analysis.

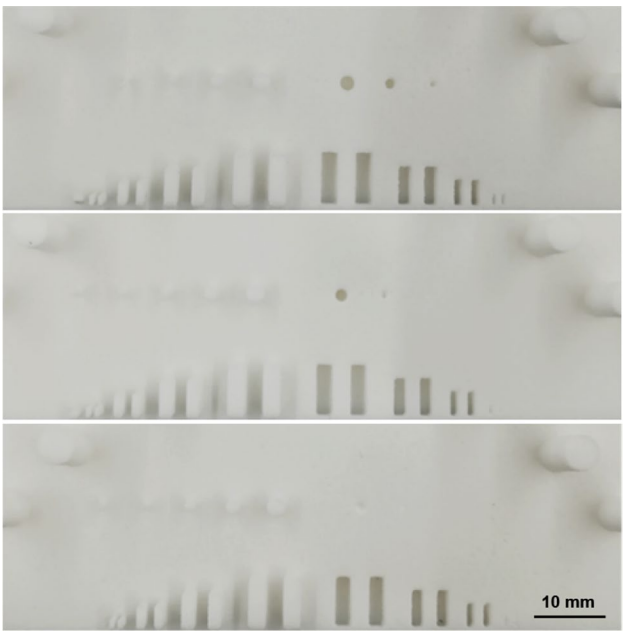

Fig. 4 Fine features of artifacts test produced by SLS with 0.198 J/mm^3 (top), 0.238 J/mm^3 (middle) and 0.278 J/mm^3 (bottom)

3.1.2 Dimensional and geometric accuracy

The evaluation of the dimensional and geometric accuracy of the artifacts test encompassed the qualitative analysis of

Fig. 5 Surface of an artifact test produced by SLS with 0.358 J/mm^3 (after sand blasting)

the CT images combined with the basic principles of Geometric Dimensioning and Tolerancing (GD&T), including the analysis of the form of single features and orientation of features in relation to others using datum reference frames [42]. The CT images revealed in detail the observations reported in the previous section concerning the brittleness of fine pins, quality of holes, surface roughness and straightness of edges, depending on ED_V (Figs. 6 and 7). These differences had a critical influence on the GD&T measurements, with particular effect on the flatness, straightness and parallelism of surfaces.

As a result of the enhanced heat conduction to the surrounding powder particles and the warping effects coming from the sintering process conducted under high levels of energy, the findings proved that low ED_V values are advantageous to produce flat surfaces (Fig. 8). Until 0.238 J/mm^3, the artifacts test presented a flatness between 0.10 mm and 0.20 mm (on average), with the highest value for 0.158 J/mm^3 reflecting the high surface roughness of the surface (see Fig. 6). A rising trend was verified after that level with values of flatness above 0.30 mm in the artifact test produced with 0.318 J/mm^3.

The artifacts test produced with low to medium levels of energy reached similar values of straightness of the primary surface, registering average values close to 0.18 mm (Fig. 9). However, a significant increase was verified in artifacts test produced with high ED_V values, reaching a maximum of 0.30 mm with 0.318 J/mm^3.

The parallelism of opposite surfaces was the GD&T function most influenced by the ED_V value (Fig. 10). The results indicated that low ED_V values are advantageous to produce parallel surfaces. In a variation of 0.16 J/mm^3, the parallelism of opposite surfaces increased more than 4 times, from 0.10 mm in the artifact test produced with 0.158 J/mm^3 to above 0.40 mm in the artifact test produced with 0.318 J/mm^3. This agrees with the results of flatness

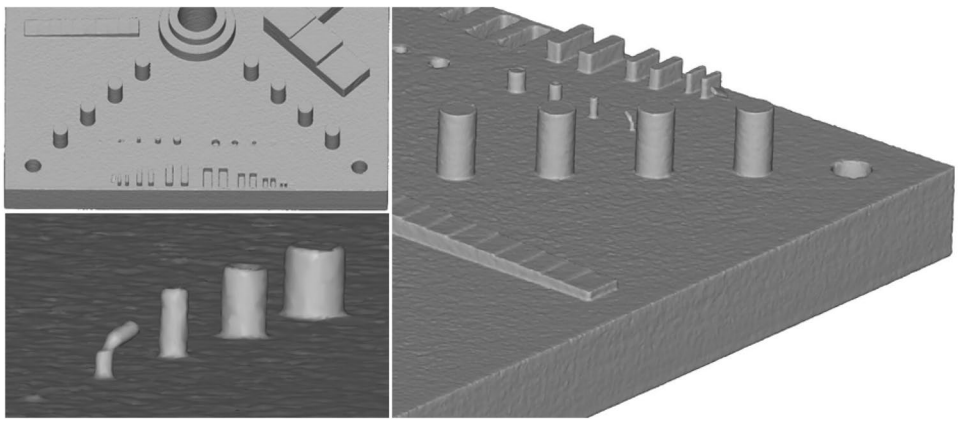

Fig. 6 CT images of an artifact test produced by SLS with 0.158 J/mm^3

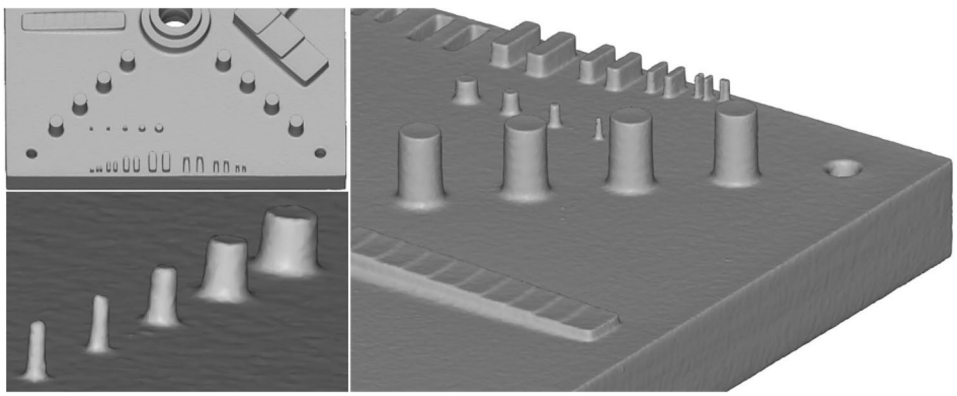

Fig. 7 CT images of an artifact test produced by SLS with 0.318 J/mm^3

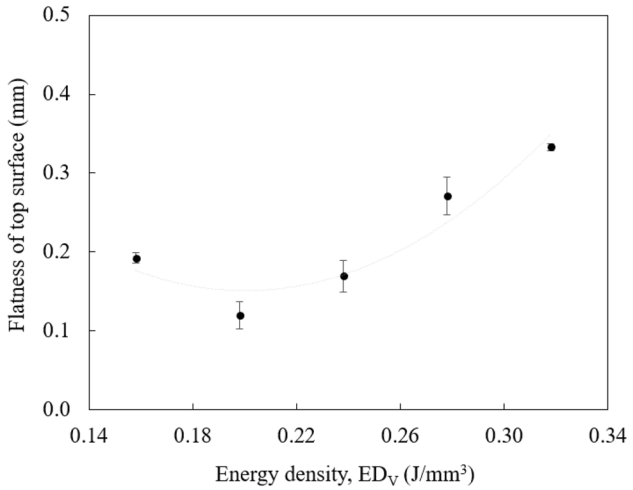

Fig. 8 Flatness of top surface of artifacts test produced by SLS depending on ED_V (XY-A strategy)

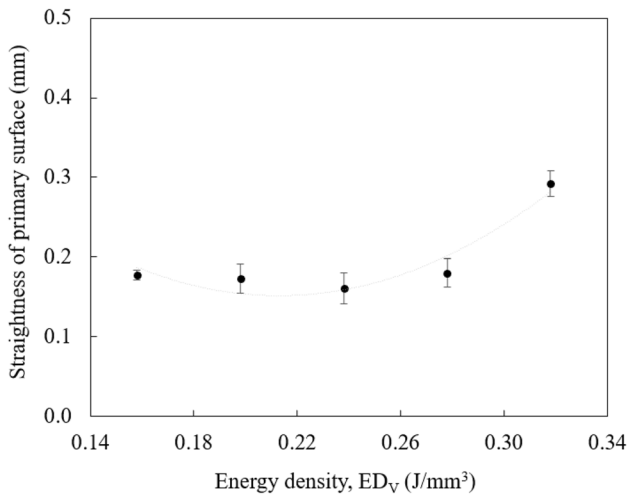

Fig. 9 Straightness of primary surface of artifacts test produced by SLS depending on ED_V (XY-A strategy)

previously discussed since the parallelism tends to increase when opposite surfaces that are not completely flat are under consideration, in consequence of the thermal conduction empowered to the surrounding powder particles.

The analysis of the dimensional accuracy of pins and holes with nominal diameters of 2.00 mm, 1.50 mm, 1.00 mm, 0.50 mm and 0.25 mm is reported in Fig. 11. The results showed that all ED_V values considered for dimensional and geometric evaluation (i.e., from 0.158 to 0.318 J/mm^3) can produce pins until a minimum of 1.00 mm of nominal diameter. Pins with 0.50 mm and 0.25 mm of nominal diameter were not produced with low ED_V values (i.e., 0.158 J/mm^3 and 0.198 J/mm^3). Despite the capability to manufacture the pins, the results showed

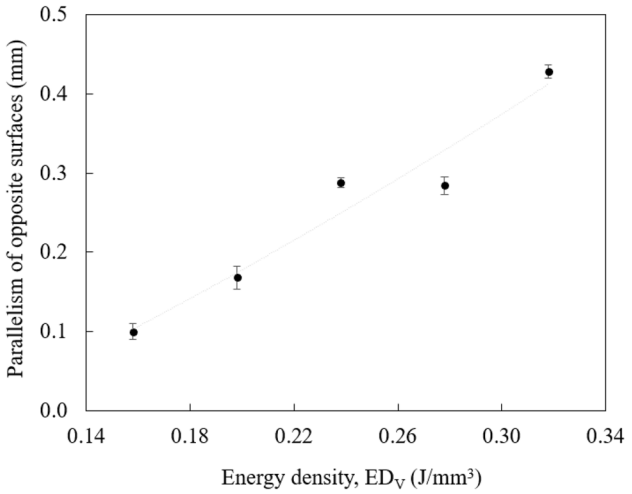

Fig. 10 Parallelism of opposite surfaces of artifacts test produced by SLS depending on ED_V (XY-A strategy)

that its diameter tends to gradually increase with ED_V. In this way, the artifact test produced with 0.158 J/mm^3 exhibited the highest deviation to a minimum value until 0.13 mm below the nominal, while the artifact test produced with 0.318 J/mm^3 exhibited the highest deviation to a maximum value until 0.17 mm above the nominal. Therefore, the medium ED_V value of 0.238 J/mm^3 was the most appropriate to produce fine pins with acceptable dimensional accuracy. Regardless of the value of energy, the minimum pin size achievable by the laser-sintering system was 0.50 mm, assuming an adequate tolerance. Below 0.50 mm, the deviations exceeded 0.30 mm.

Opposite trends were verified for the holes. In this regard, ED_V values above 0.238 J/mm^3 were not able to produce fine holes with a nominal diameter equal to or less than 2.00 mm. As opposed to the pins, the average diameter of the holes tends to gradually decrease with ED_V. For instance, the ED_V of 0.238 J/mm^3 was only able to produce holes until a nominal diameter of 1.50 mm, with a maximum deviation of 0.62 mm below the nominal. In turn, ED_V values of 0.198 J/mm^3 and 0.158 J/mm^3 were able to produce holes until a nominal diameter of 1.00 mm, with a maximum deviation until 0.26 mm and 0.10 mm below the nominal, respectively. Therefore, the lowest ED_V value of 0.158 J/mm^3 was the most suitable to produce fine holes until 1.00 mm with satisfactory dimensional accuracy.

The dimensional and geometric evaluation of the artifacts test produced with 0.318 J/mm^3 using different laser beam strategies showed some differences in the quality of the surfaces and edges, with particular effect on the flatness, straightness and parallelism. The results evidenced that the XY-A and Y strategies allow the production of SLS parts with similar geometric characteristics. However, the artifacts test produced with the X strategy presented

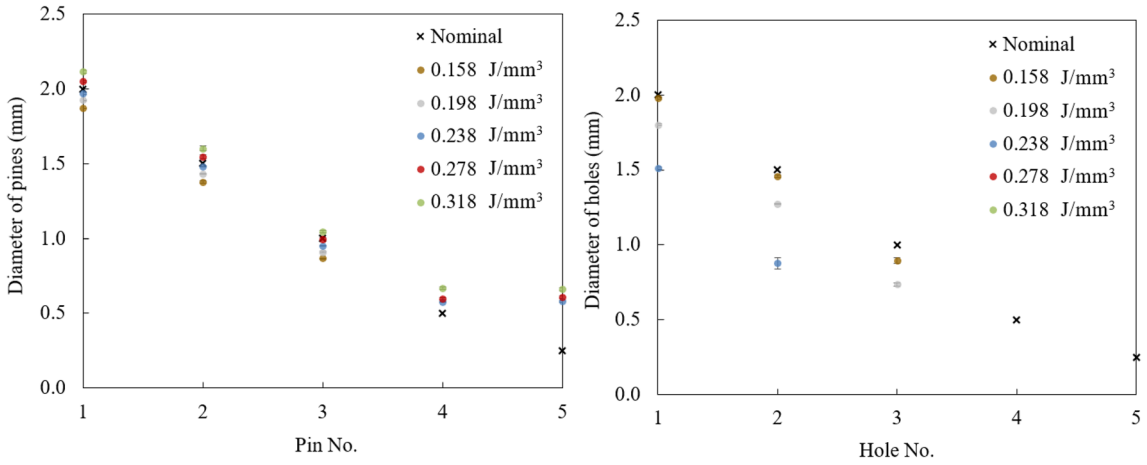

Fig. 11 Diameter of pins (left) and holes (right) of artifacts test produced by SLS depending on ED_V (XY-A strategy)

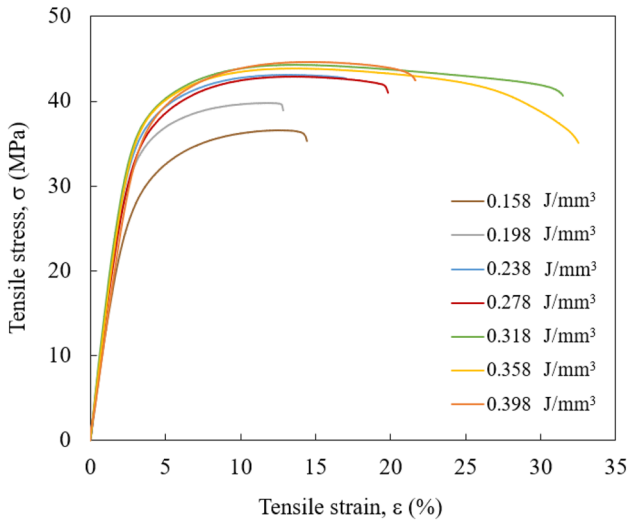

Fig. 12 Typical engineering stress–strain curves of test specimens produced by SLS depending on ED_V (XY-A strategy)

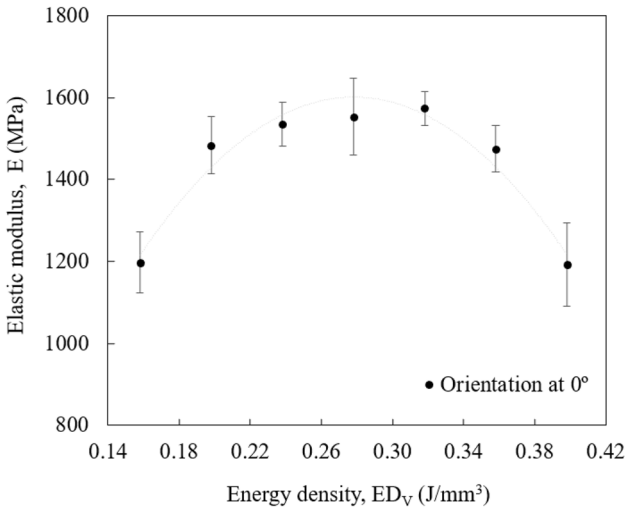

Fig. 13 Elastic modulus of test specimens produced by SLS depending on ED_V (XY-A strategy)

greater quality by obtaining flat, straight and parallel surfaces.

3.1.3 Mechanical properties

The mechanical analysis demonstrated the significant effect of ED_V on the mechanical performance of the test specimens produced by SLS with a single exposure type through the modification of the hatching parameters, as evidenced in typical engineering stress–strain curves obtained from the experiments (Fig. 12).

Regarding the elastic modulus, it was verified that it increased from low to medium values of energy and decreased from medium to high values of energy, recording 1197.0 ± 74.2 MPa with 0.158 J/mm^3, 1553.6 ± 93.3 MPa with 0.278 J/mm^3 and 1192.7 ± 100.8 MPa with 0.398 J/mm^3 (Fig. 13).

The tensile stress at yield also increased with ED_V, recording a difference of 38% in 0.24 J/mm^3 [Fig. 14 (left)]. For instance, the test specimens produced with 0.158 J/mm^3 recorded 22.1 ± 1.2 MPa and the test specimens produced with 0.398 J/mm^3 recorded 30.5 ± 1.3 MPa. The tensile stress at break did not exhibit a relevant trend with ED_V, registering values between 35 and 41 MPa [Fig. 14 (right)].

The tensile strain at yield had a non-sensitive effect in test specimens produced with medium–low values of energy [Fig. 15 (left)]. However, it significantly increased with high levels. The tensile strain at break also showed an increasing trend with ED_V [Fig. 15 (right)]. These results, combined with the large plastic region evidenced on the corresponding

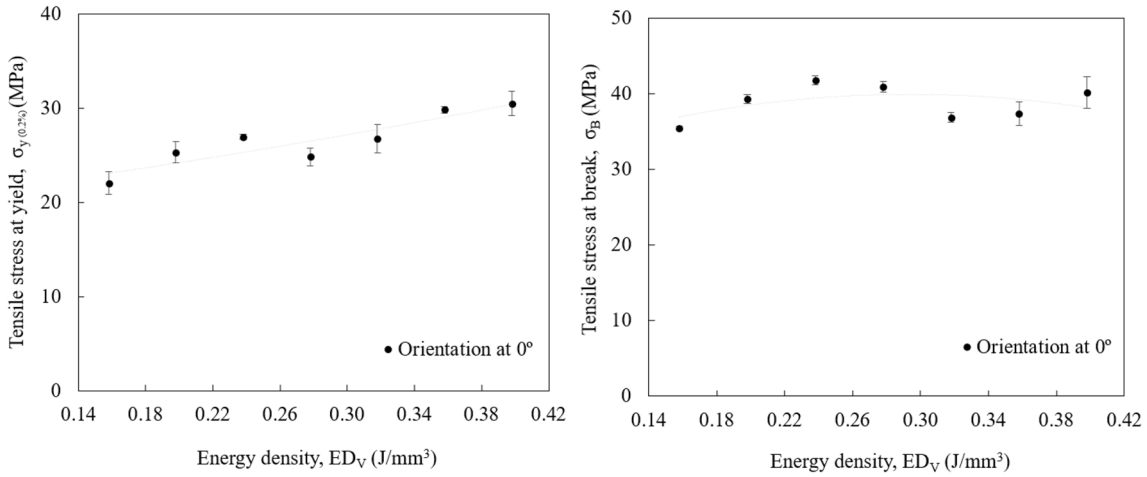

Fig. 14 Tensile stress at yield (left) and tensile stress at break (right) of test specimens produced by SLS depending on ED_V (XY-A strategy)

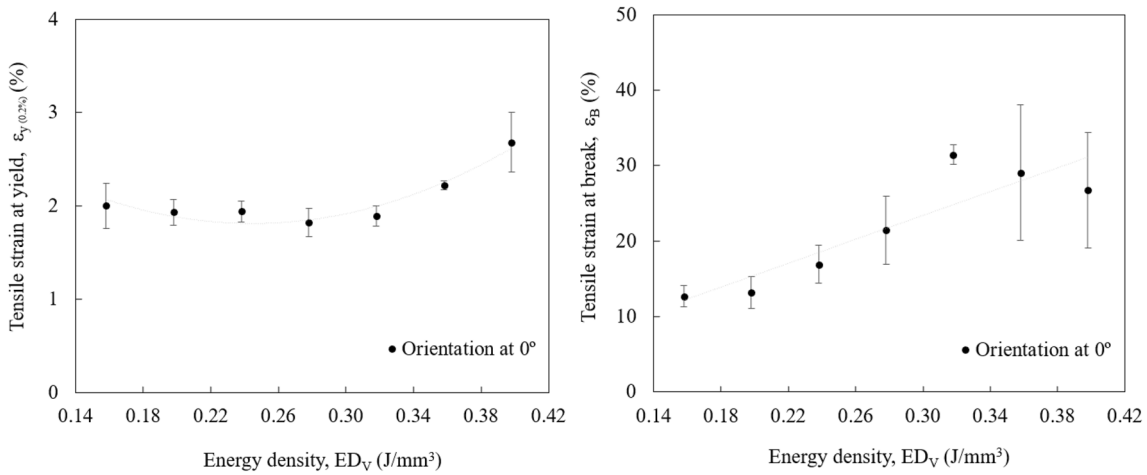

Fig. 15 Tensile strain at yield (left) and tensile strain at break (right) of test specimens produced by SLS depending on ED_V (XY-A strategy)

stress–strain curves, prove that SLS parts become less brittle when the sintering process is conducted with high ED_V values [16].

The tensile strength increased with ED_V to a great extent from 0.158 to 0.318 J/mm^3, achieving a maximum variation of 22.0% (Fig. 16). After the rising trend until medium–high levels of energy, an asymptotic value close to 44 MPa was reached with a variation of less than 1.0% between experiments. This output, as well as the results of tensile stress at yield, evidenced that medium–high levels of energy are desired to improve the mechanical strength of SLS parts above 20.0%. This increasing trend until values between 40 and 50 MPa is in agreement with similar experiments reported in literature, despite the slight difference in the level of energy at which properties stabilization begins [10].

In respect of the strategy of the laser beam, the mechanical analysis showed that the highest values of tensile stress at yield, tensile stress at break and tensile strength were obtained in the test specimens produced with the laser beam operating in the *y*-direction. For instance, the tensile strength of the test specimens produced with this laser beam path was 9.8% higher compared with the standard XY-A strategy (i.e., from 44.1 ± 1.0 to 48.4 ± 1.0 MPa) (Fig. 17).

3.1.4 Morphological properties

Figure 18 shows SEM micrographs of the cross-section of test specimens produced by SLS with low (i.e., 0.158 J/mm^3), medium (i.e., 0.278 J/mm^3) and high (i.e., 0.358 J/mm^3) values of energy, using the XY-A strategy of the laser beam path.

The micro-scale images illustrate that the test specimens produced with low ED_V values exhibited large voids and gaps between the layers of powder due to the insufficient

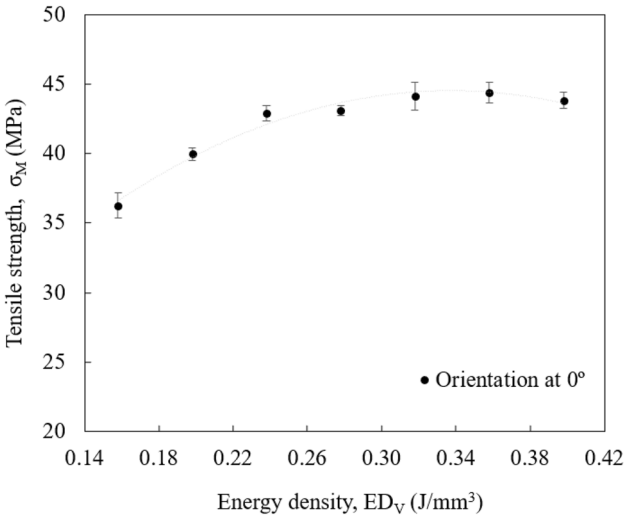

Fig. 16 Tensile strength of test specimens produced by SLS depending on ED_V (XY-A strategy)

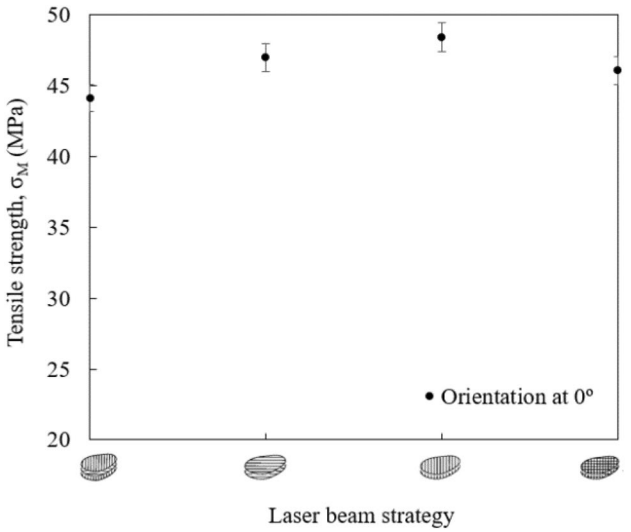

Fig. 17 Tensile strength of test specimens produced by SLS depending on the hatching strategy (0.318 J/mm^3)

energy density supplied by the laser beam, which is an essential condition for an efficient inter-particle consolidation. In turn, the cross-section of the test specimens became more homogeneous with less content of porosity when medium–high levels of energy were considered for the sintering. However, an intensive exposure of the powder particles to the laser beam operating with excessive levels of energy resulted in a damaged cross-section, with voids reaching 160 µm of diameter (on average). These morphological characteristics had a critical effect on the mass and mechanical properties of the test specimens, explaining the reduction of the tensile strength from 36.2 ± 0.9 MPa in test specimens produced with low ED_V values to 44.4 ± 0.7 MPa in test specimens produced with medium–high ED_V values. The strategy of the laser beam did not induce significant morphological differences in the cross-section of the test specimens, comparing with the effect of ED_V.

3.2 Single exposure type of contour parameters

The experiments conducted to evaluate the contour parameters using a single exposure type proved that the properties of SLS parts are more influenced by the hatching parameters defining the largest portion of its bulk volume. In fact, the morphological analysis did not reveal significant differences between hatching and contour layers, explaining the low dimensional, geometric and mechanical variations obtained in the experiments. However, the test specimens produced with 0.007 J/mm exhibited slight benefits in relation to the others. They presented the lowest values of flatness (i.e., 0.23 ± 0.01 mm), straightness (i.e., 0.23 ± 0.02 mm) and parallelism (i.e., 0.29 ± 0.01 mm) and the highest values of tensile stress at yield (i.e., 37.2 ± 2.3 MPa), tensile stress at break (i.e., 50.5 ± 0.5 MPa) and tensile strength (i.e., 55.6 ± 0.8 MPa). In fact, a medium–high ED_V value defined for the hatching combined with a low ED_V value defined for the contour was advantageous to maximize the overall performance of the test specimens, ensuring a valuable compromise between strength and accuracy.

3.3 Multiple exposure type using a skin/core configuration

The individual analysis of hatching and contour parameters revealed that when the energy provided during the sintering process is high, the heat conduction empowers the secondary sintering of surrounding powder particles, improving the mechanical properties but reducing the dimensional and geometric accuracy of the parts. This means that medium–high ED_V values are beneficial for mechanical strength, while medium–low ED_V values are preferable for surface finishing and dimensional and geometric accuracy of features. Based on these assumptions, this section focuses on the production of tests specimens with 0.318 J/mm^3 supplied to the core and 0.198 J/mm^3 supplied to the skin, defining 20%, 30% and 40% of the t_{Part} (Table 4).

3.3.1 Description of observations

The qualitative analysis of the artifacts test produced with a multiple exposure type revealed the first benefits of the skin/core configuration. While the artifact test entirely produced with 0.318 J/mm^3 using a single exposure type did not exhibit fine holes equal to or less than 2.00 mm of nominal diameter, fine holes until 1.00 mm were detectable on the

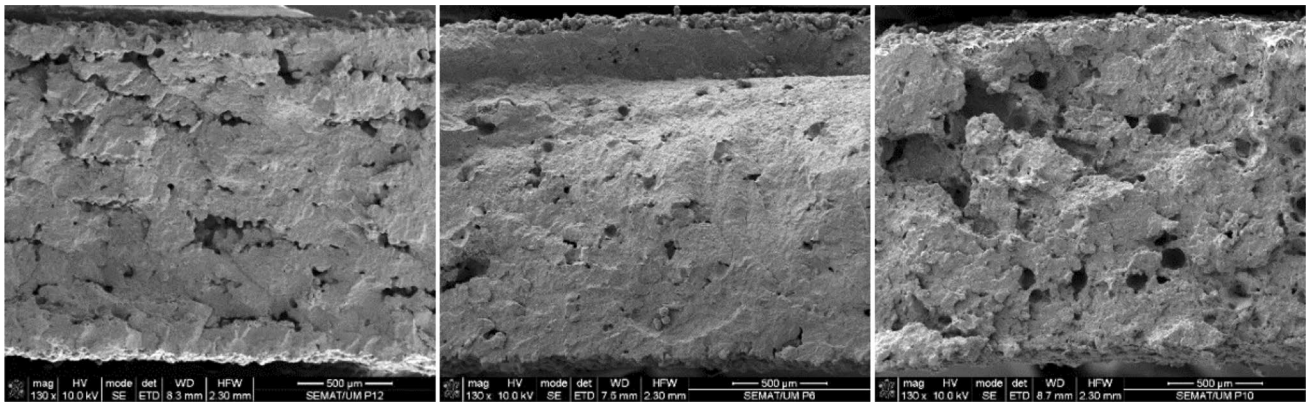

Fig. 18 Cross-section of test specimens produced by SLS with 0.158 J/mm^3 (left), 0.278 J/mm^3 (middle) and 0.358 J/mm^3 (right) (XY-A strategy)

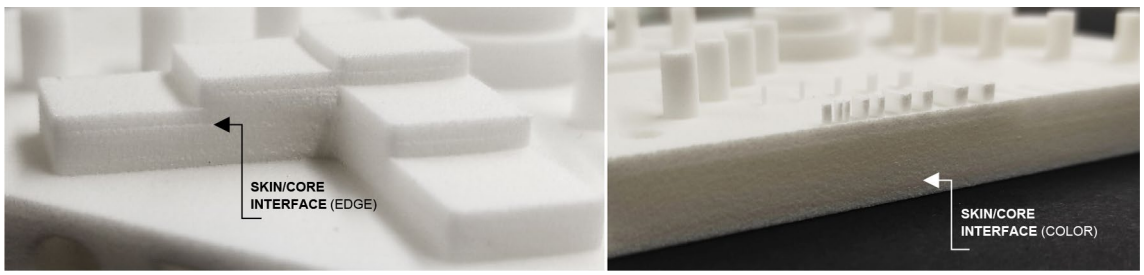

Fig. 19 Details of an artifact test produced by SLS with combination of parameters

top surface of the artifacts test produced with the advanced parameterization mode. However, in consequence of the substantial difference of energy density involved, a clear interface between the layers defining the skin and the core through an additional edge and slight differences of color was visible on the features and surfaces of the artifacts test (Fig. 19).

3.3.2 Dimensional and geometric accuracy

The CT images of the artifacts test produced with the combination of parameters revealed in detail the observations reported in the previous section that induced significant differences in the GD&T measurements. As stated before for the single exposure types, one of the GD&T basics most influenced by the operating settings is flatness. In this respect, the dimensional and geometric analysis showed that the flatness of parts produced by SLS with 0.318 J/mm^3 can be reduced until 26.1% (i.e., decreasing from 0.23 to 0.17 mm (on average)) when skin layers sintered with 0.198 J/mm^3 defining 40% of the t_{Part} are included (Fig. 20).

The straightness of the primary surface also showed a strong dependence on the skin/core combination (Fig. 21). While the artifacts test entirely produced with 0.318 J/mm^3

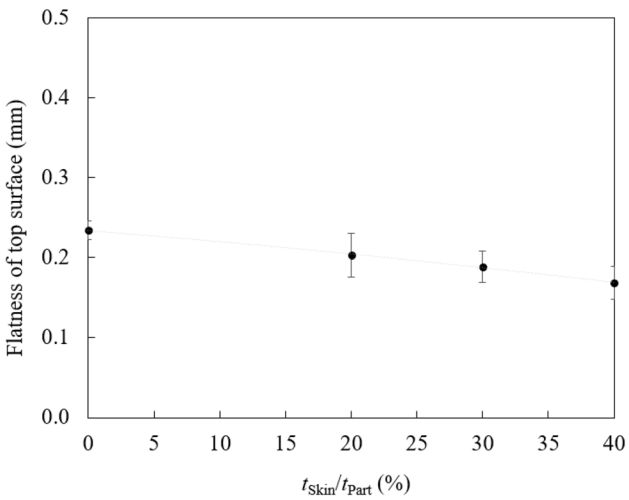

Fig. 20 Flatness of top surface of artifacts test produced by SLS with combination of parameters

presented straightness above 0.20 mm, the inclusion of skin layers sintered with 0.198 J/mm^3 allowed a reduction to 0.14–0.18 mm, regardless of the t_{Skin}.

As expected, the parallelism decreased from 0.44 to 0.29 mm in artifacts test produced with the t_{Skin} increasing

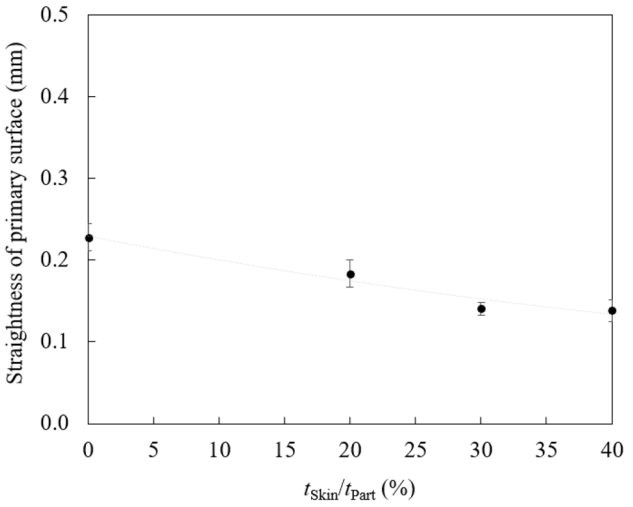

Fig. 21 Straightness of primary surface of artifacts test produced by SLS with combination of parameters

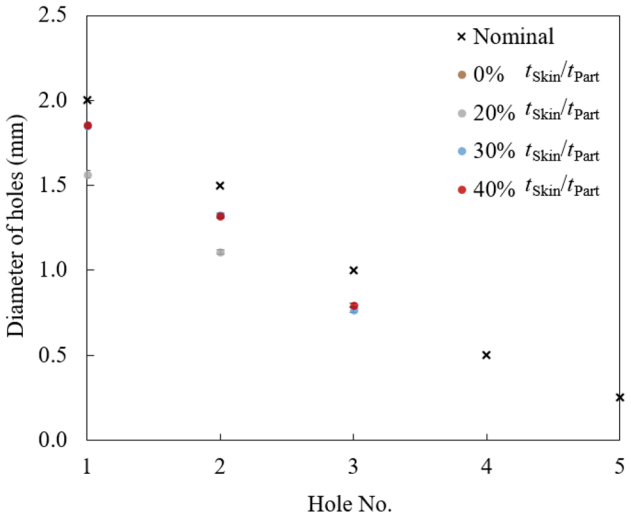

Fig. 23 Diameter of holes of artifacts test produced by SLS with combination of parameters

from 20% to 40% of the t_{Part}, respectively, in function of the overall ED_V (Fig. 22). However, the artifact test produced with 0% of t_{Skin} recorded the lowest value of 0.29 mm. This proved that the physical interface observed between the skin and core layers preventing the production of flat lateral surfaces, as illustrated in Fig. 22, had a negative effect on the dimensional and geometric accuracy of the primary surfaces of the artifact test.

The findings concerning the fine pins were coherent with the results reported in Fig. 11. The CT analysis demonstrated that the experiments with 0% and 20% of t_{Skin}/t_{Part} ensure similar outputs, while the experiments with 30% and 40% of t_{Skin}/t_{Part} exceed deviations of 0.10 mm in all fine pins. Within the scope of fine features, the greatest benefits of the multiple exposure type were in the manufacturing of holes that were not observed in artifacts test produced with 0% of t_{Skin} (Fig. 23). In this regard, the condition of 20% of t_{Skin}/t_{Part} allowed the production of fine holes until 1.50 mm, while the conditions of 30% and 40% of t_{Skin}/t_{Part} allowed the production of fine holes until 1.00 mm of nominal diameter. However, a satisfactory dimensional tolerance below 0.10 mm was not guaranteed in any experiment.

3.3.3 Mechanical properties

The engineering stress–strain curves obtained from the tensile tests revealed that the mechanical properties of the test specimens decreased when skin layer sintered with low values of energy were combined with a medium–high level of energy defined for the core (Fig. 24).

The reduction of the mechanical properties was observed in the elastic modulus and tensile strength. The elastic modulus decreased from 1674.5 ± 77.7 MPa in test specimens produced with a single exposure type to values ranging from

Fig. 22 Parallelism of opposite surfaces of artifacts test produced by SLS with combination of parameters

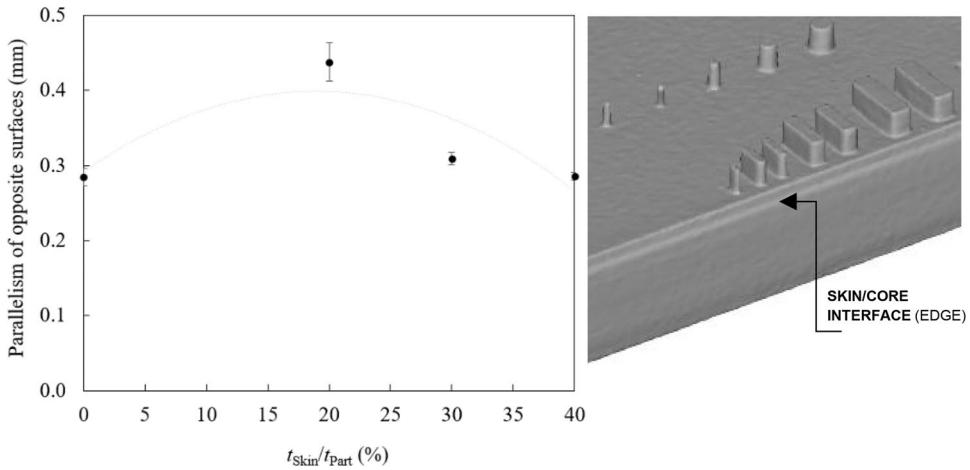

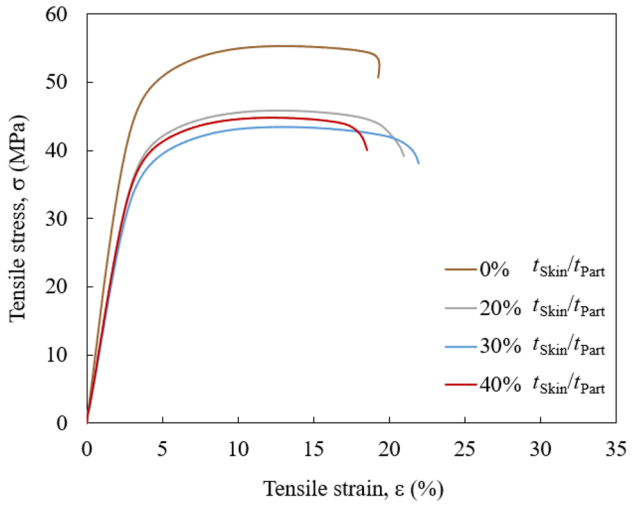

Fig. 24 Typical engineering stress–strain curves of test specimens produced by SLS depending on the combination of parameters

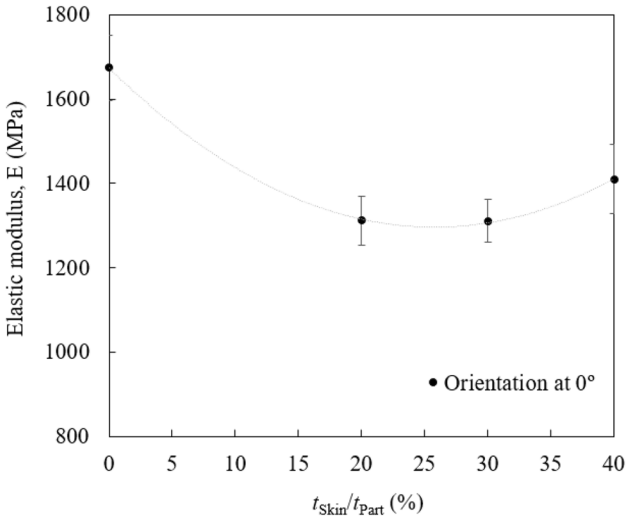

Fig. 25 Elastic modulus of test specimens produced by SLS depending on the combination of parameters

1311.6 to 1409.7 MPa in test specimens produced with the combination of parameters (Fig. 25). This occurs due to the increased number of layers sintered with low values of energy that induce reduced values of elastic modulus, evidencing few brittle characteristics (see Fig. 13).

The tensile stress at yield gradually decreased from 37.2 ± 2.3 MPa in test specimens produced without the combination of parameters to a minimum of 31.1 ± 1.0 MPa in test specimens produced with 40% of t_{Skin}/t_{Part}, recording a reduction of 16.4% (Fig. 26 (left)). Similar outputs were verified for the tensile stress at break which reduced 19.2% from 50.5 ± 1.1 MPa in test specimens produced without combination of parameters to 40.8 ± 0.9 MPa in test specimens produced with 40% of t_{Skin}/t_{Part} [Fig. 26 (right)].

The results of tensile strain at yield and tensile strain at break [Fig. 27 (left and right, respectively)], did not reveal a significant variation with the t_{Skin}/t_{Part} relationship, recording values similar to those obtained in the test specimens entirely produced with 0.318 J/mm^3. These results combined with the evolution of typical engineering stress–strain curves (Fig. 25) suggest that when a combined parameterization mode is applied, the test specimens require inferior mechanical load to induce similar strain levels, due to their more ductile behavior (i.e., reduced elastic modulus).

Furthermore, the tensile strength reached a maximum reduction of 20.3% from 55.6 ± 0.8 MPa using the standard parameterization mode to values ranging between 44.3–46.0 MPa using the combined method (Fig. 28).

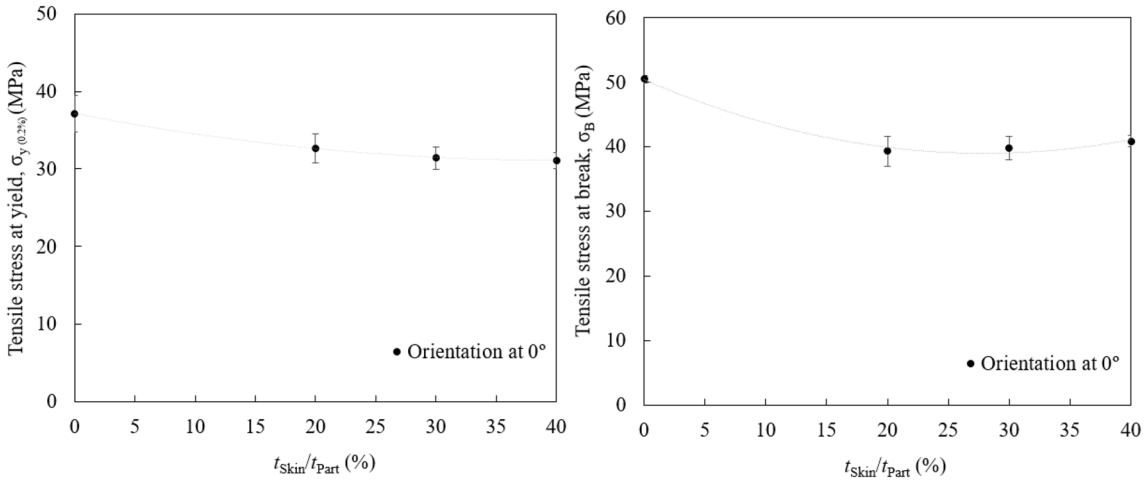

Fig. 26 Tensile stress at yield (left) and tensile stress at break (right) of test specimens produced by SLS depending on the combination of parameters

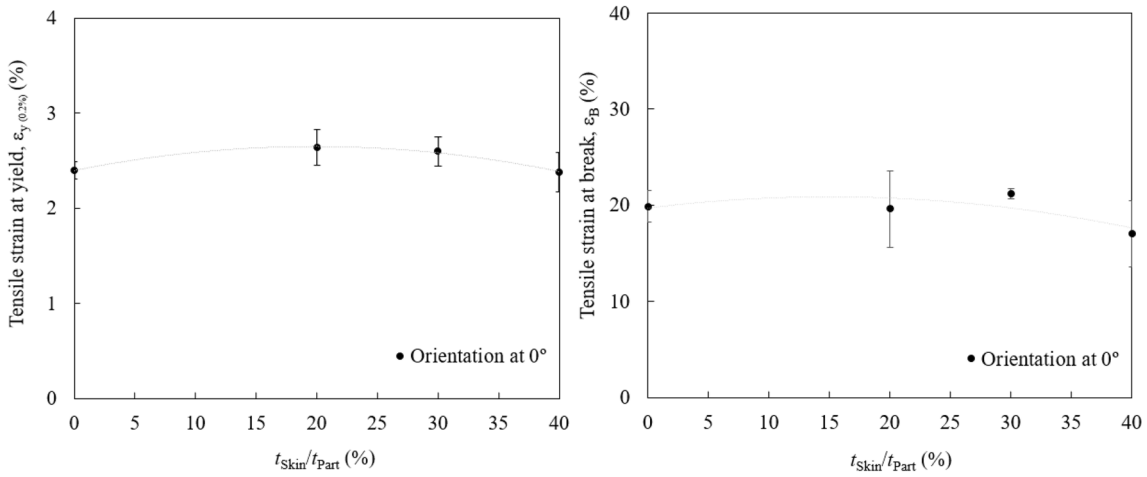

Fig. 27 Tensile strain at yield (left) and tensile strain at break (right) of test specimens produced by SLS depending on the combination of parameters

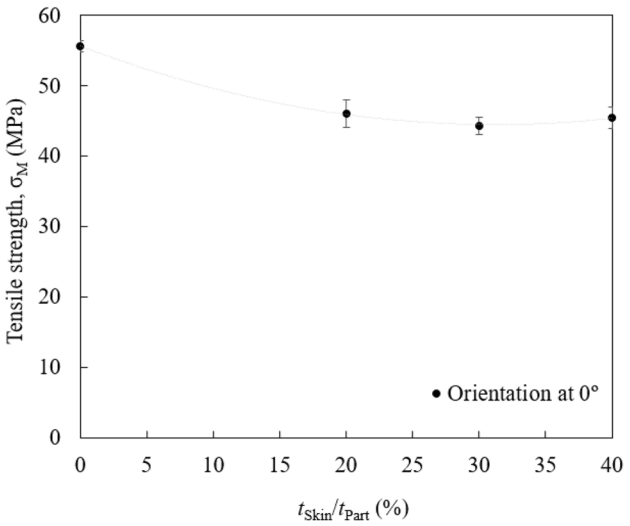

Fig. 28 Tensile strength of test specimens produced by SLS depending on the combination of parameters

3.3.4 Morphological properties

The SEM micrographs of the cross-section of test specimens produced by SLS with a multiple exposure type showed that the cross-section of the test specimens presented high content of porosity with voids reaching an average of 150 µm of diameter (Fig. 29). However, the micrographs did not reveal clear differences between the layers defining the skin and core configurations, neither significant modifications in the cross-section of the test specimens produced with different t_{Skin}/t_{Part} relationships. This suggests that the morphological structure of SLS parts is mostly governed by the ED_V value supplied for the hatching layers. With these findings, it is possible to argue that the intrinsic porosity of SLS parts can be controlled in advance with proper adjustment of hatching parameters to provide medium–high ED_V values to their internal layers (see Fig. 18).

Despite the almost insensitive morphological modifications, this section showed that the implementation of a multiple exposure type influences the properties of SLS parts, in terms of mechanical strength and overall accuracy. Although different process parameters are required to optimize these non-compatible properties, a promising balance can be established using a combined parameterization mode. In this research, improvements in the flatness and straightness of surfaces and the manufacture of fine holes were reached using an advanced parameterization method, with an average reduction of 20% in the mechanical properties. The achievements proved that the definition of the optimum set of process parameters for each building job, whether in single or combined approaches, strongly depends on the part and its technical specifications.

4 Conclusion

The influence of the thermal energy supplied by the laser beam to the powder particles during the sintering on the overall performance of parts produced by SLS was evaluated in this research using single and multiple exposure types. The experiments demonstrated that medium–low ED_V values, from 0.158 to 0.238 J/mm^3, supplied to the hatching layers are desirable to ensure great dimensional and geometric outputs while medium–high ED_V values, from 0.278 to 0.318 J/mm^3, are desirable to maximize the mechanical properties of the parts. Above 0.318 J/mm^3, the process becomes unfeasible due to the excessive level of energy and negative effects induced by the secondary sintering. In this

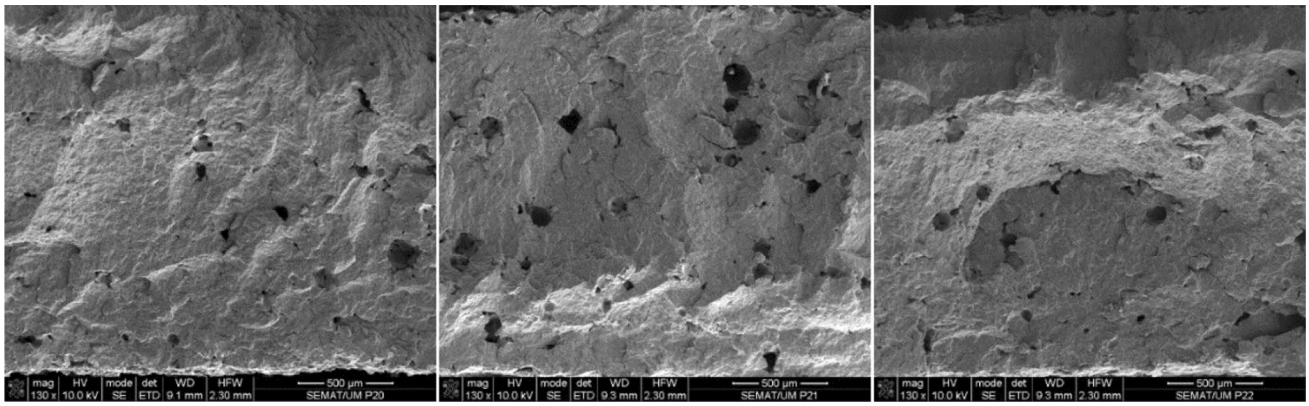

Fig. 29 Cross-section of test specimens produced by SLS with 20% (left), 30% (middle) and 40% (right) of t_{Skin}/t_{Part}

research, this phenomenon had significant influence on the dimensional accuracy of the parts with the increasing level of energy. Regardless of the ED_V value, it was proved that preference should be given to the *xy*-alternating-direction and *y*-direction strategies of the laser beam, rather than the *xy*-simultaneous-direction and *x*-direction. As opposed to the hatching, the variation of the contour parameters using a single exposure type, from low to high values of energy, did not have a significant effect on the main properties of the parts. On the other hand, the valuable potential in combining different process parameters defining a skin/core configuration was showed. In this regard, promising values of flatness and straightness of surfaces were allowed without significant loss of mechanical properties. To conclude, it was proved that an in-depth understanding of the individual effect of fundamental SLS process parameters makes it possible for the implementation of a multiple exposure type with the potential to ensure a set of properties suited to technical requirements. This knowledge base combined with analytical solutions describing the experimental process-structure–property relationship are useful insights to monitor the sintering process by estimating the properties of the parts as a function of the process parameters. Other exposure types will be explored in future work to enhance the competitiveness of SLS, in relation to conventional processing technologies.

Author contributions Not applicable.

Funding This work was co-funded by the European Regional Development Fund through the Operational Competitiveness and Internationalization Programme (COMPETE 2020) [Project No. 47108, "SIFA"; Funding Reference: POCI-01-0247-FEDER-047108] and by the Foundation for Science and Technology (FCT) through the PhD scholarship 2020.04520.BD.

Availability of data and material Not applicable.

Code availability Not applicable.

Declarations

Conflict of interest The authors have no conflicts of interest to declare.

References

1. ASTM (2012) ASTM F2792 12a - Standard Terminology for Additive Manufacturing Technologies
2. Chatham CA, Long TE, Williams CB (2019) A review of the process physics and material screening methods for polymer powder bed fusion additive manufacturing. Prog Polym Sci 93:68–95. https://doi.org/10.1016/j.progpolymsci.2019.03.003
3. Wörz A, Wudy K, Drummer D et al (2018) Comparison of long-term properties of laser sintered and injection molded polyamide 12 parts. J Polym Eng 38:573–582. https://doi.org/10.1515/polyeng-2017-0227
4. Kumar S (2003) Selective laser sintering: a qualitative and objective approach. J Miner Met Mater Soc 55:43–47
5. Bourell DL, Watt TJ, Leigh DK, Fulcher B (2014) Performance limitations in polymer laser sintering. Phys Procedia 56:147–156. https://doi.org/10.1016/j.phpro.2014.08.157
6. Gibson I, Rosen D, Stucker B (2010) Powder bed fusion processes. In: Additive manufacturing technologies - rapid prototyping to direct digital manufacturing. Springer International Publishing, Boston, pp 103–142
7. Duan B, Wang M (2011) Selective laser sintering and its application in biomedical engineering. MRS Bull 36:998–1005. https://doi.org/10.1557/mrs.2011.270
8. Pavan M, Faes M, Strobbe D et al (2017) On the influence of inter-layer time and energy density on selected critical-to-quality properties of PA12 parts produced via laser sintering. Polym Test 61:386–395. https://doi.org/10.1016/j.polymertesting.2017.05.027
9. Pilipović A, Drstvenšek I, Šercer M et al (2014) Mathematical model for the selection of processing parameters in selective laser sintering of polymer products. Adv Mech Eng. https://doi.org/10.1155/2014/648562
10. Hofland EC, Baran I, Wismeijer DA (2017) Correlation of process parameters with mechanical properties of laser sintered PA12 parts. Adv Mater Sci Eng. https://doi.org/10.1155/2017/4953173
11. Kiani A, Khazaee S, Badrossamay M et al (2020) An investigation into thermal history and its correlation with mechanical properties of PA12 parts produced by selective laser sintering process. J Mater Eng Perform 29:832–840. https://doi.org/10.1007/s11665-020-04640-0

12. Majewski C, Zarringhalam H, Hopkinson N (2008) Effect of the degree of particle melt on mechanical properties in selective laser-sintered Nylon-12 parts. Proc Inst Mech Eng Part B J Eng Manuf 222:1055–1064. https://doi.org/10.1243/09544054JEM1122
13. Amado-Becker A, Ramos-Grez J, José Yañez M et al (2008) Elastic tensor stiffness coefficients for SLS Nylon 12 under different degrees of densification as measured by ultrasonic technique. Rapid Prototyp J 14:260–270. https://doi.org/10.1108/13552540810907929
14. Beitz S, Uerlich R, Bokelmann T et al (2019) Influence of powder deposition on powder bed and specimen properties. Materials. https://doi.org/10.3390/ma12020297
15. Shi D, Gibson I (1997) Material properties and fabrication parameters in selective laser sintering process. Rapid Prototyp J 3:129–136. https://doi.org/10.1108/13552549710191836
16. Caulfield B, McHugh PE, Lohfeld S (2007) Dependence of mechanical properties of polyamide components on build parameters in the SLS process. J Mater Process Technol 182:477–488. https://doi.org/10.1016/j.jmatprotec.2006.09.007
17. Beard MA, Ghita OR, Evans KE (2011) Monitoring the effects of selective laser sintering (SLS) build parameters on polyamide using near infrared spectroscopy. J Appl Polym Sci 121:3153–3158
18. Tong Q, Xue K, Wang T, Yao S (2020) Laser sintering and invalidating composite scan for improving tensile strength and accuracy of SLS parts. J Manuf Process 56:1–11. https://doi.org/10.1016/j.jmapro.2020.04.056
19. Czelusniak T, Amorim FL (2020) Influence of energy density on selective laser sintering of carbon fiber-reinforced PA12. Int J Adv Manuf Technol 111:2361–2376. https://doi.org/10.1007/s00170-020-06261-2
20. Chunze Y, Yusheng S, Zhaoqing L et al (2020) Selective laser sintering forming accuracy control. In: selective laser sintering additive manufacturing technology. Academic Press, Cambridge, pp 671–716
21. Ho HCH, Gibson I, Cheung WL (1999) Effects of energy density on morphology and properties of selective laser sintered polycarbonate. J Mater Process Technol 89–90:204–210. https://doi.org/10.1016/S0924-0136(99)00007-2
22. Dewulf W, Pavan M, Craeghs T, Kruth J-P (2016) Using X-ray computed tomography to improve the porosity level of polyamide-12 laser sintered parts. CIRP Ann Manuf Technol 65:205–208. https://doi.org/10.1016/j.cirp.2016.04.056
23. Wu J, Xu X, Zhao Z et al (2018) Study in performance and morphology of polyamide 12 produced by selective laser sintering technology. Rapid Prototyp J 24:813–820. https://doi.org/10.1108/RPJ-01-2017-0010
24. Ling Z, Wu J, Wang X et al (2018) Experimental study on the variance of mechanical properties of polyamide 6 during multi-layer sintering process in selective laser sintering. Int J Adv Manuf Technol 6:1–8. https://doi.org/10.1007/s00170-018-3004-8
25. Kummert C, Schmid HJ (2018) The Influence of Contour Scanning Parameters and Strategy on Selective Laser Sintering PA613 Build Part Properties. Proc 29th Annu Int Solid Free Fabr Symp 1582–1591
26. Beal VE, Paggi RA, Salmoria GV, Lago A (2009) Statistical evaluation of laser energy density effect on mechanical properties of polyamide parts manufactured by selective laser sintering. J Appl Polym Sci 113:2910–2919
27. Bacchewar PB, Singhal SK, Pandey PM (2007) Statistical modelling and optimization of surface roughness in the selective laser sintering process. Proc Inst Mech Eng Part B J Eng Manuf 221:35–52. https://doi.org/10.1243/09544054JEM670
28. Goodridge RD, Tuck CJ, Hague RJM (2012) Laser sintering of polyamides and other polymers. Prog Mater Sci 57:229–267. https://doi.org/10.1016/j.pmatsci.2011.04.001
29. Jain PK, Pandey PM, Rao PVM (2009) Effect of delay time on part strength in selective laser sintering. Int J Adv Manuf Technol 43:117–126. https://doi.org/10.1007/s00170-008-1682-3
30. Franco A, Lanzetta M, Romoli L (2010) Experimental analysis of selective laser sintering of polyamide powders: an energy perspective. J Clean Prod 18:1722–1730. https://doi.org/10.1016/j.jclepro.2010.07.018
31. Pilipović A, Bogdan V, Brajlih T, et al (2010) Influence of Laser Sintering Parameters on Mechanical Properties of Polymer Products. 3rd International Conference on Additive Technologies iCAT2010 Proceedings. DAAAM International, Vienna
32. Starr TL, Gornet TJ, Usher JS (2011) The effect of process conditions on mechanical properties of laser-sintered nylon. Rapid Prototyp J 17:418–423. https://doi.org/10.1108/13552541111184143
33. Wegner A, Witt G (2012) Correlation of process parameters and part properties in laser sintering using response surface modeling. Phys Procedia 39:480–490. https://doi.org/10.1016/j.phpro.2012.10.064
34. Franco A, Romoli L (2012) Characterization of laser energy consumption in sintering of polymer based powders. J Mater Process Technol 212:917–926. https://doi.org/10.1016/j.jmatprotec.2011.12.003
35. Castoro M (2013) Impact of laser power and build orientation on the mechanical properties of selectively laser sintered parts. In: Proceedings of the national conference on undergraduate research (NCUR). University of Wisconsin La Crosse, WI, 11–13 April 2013
36. Wegner A, Harder R, Witt G, Drummer D (2015) Determination of optimal processing conditions for the production of polyamide 11 parts using the laser sintering process. IJEP 3:5–12
37. Pilipović A, Brajlih T, Drstvenšek I (2018) Influence of processing parameters on tensile properties of SLS polymer product. Polymers. https://doi.org/10.3390/polym10111208
38. Lopes AC, Sampaio AM, Silva CS, Pontes AJ (2021) Prediction of SLS parts properties using reprocessing powder. Rapid Prototyp J 27:496–506. https://doi.org/10.1108/RPJ-04-2020-0076
39. EOS GmbH (2016) Printed operations manual written and provided by EOS GmbH when purchasing the SLS equipment
40. Moylan S, Slotwinski J, Cooke A et al (2014) An additive manufacturing test artifact. J Res Natl Inst Stand Technol 119:429–459
41. International Organization for Standardization (ISO) (1996) BS EN ISO 527-2:1996, BS 2782-3: Method 322: ISO 527 Plastics — Determination of tensile properties. ISO 527-2 | Section 6: Test specimens. Annex A | Small test specimens - Figure A.1
42. Puncochar DE (1997) Interpretation of geometric dimensioning and tolerancing, 3th ed. Industrial Press, Inc., New York